Inorganic Chemistry

pubs.acs.org/IC Article

Alternative Strategy to Obtain Artificial Imine Reductase by Exploiting Vancomycin/D-Ala-D-Ala Interactions with an Iridium Metal Complex

Giorgio Facchetti,[§] Raffaella Bucci,[§] Marco Fusè, Emanuela Erba, Raffaella Gandolfi, Sara Pellegrino,* and Isabella Rimoldi*

Cite This: *Inorg. Chem.* 2021, 60, 2976−2982 Read Online

ACCESS | Metrics & More | Article Recommendations | Supporting Information

ABSTRACT: Based on the supramolecular interaction between vancomycin (Van), an antibiotic glycopeptide, and D-Ala-D-Ala (DADA) dipeptides, a novel class of artificial metalloenzymes was synthesized and characterized. The presence of an iridium(III) ligand at the *N*-terminus of DADA allowed the use of the metalloenzyme as a catalyst in the asymmetric transfer hydrogenation of cyclic imines. In particular, the type of link between DADA and the metal-chelating moiety was found to be fundamental for inducing asymmetry in the reaction outcome, as highlighted by both computational studies and catalytic results. Using the [IrCp*(*m*-I)Cl]Cl ⊂ Van complex in 0.1 M CH_3COONa buffer at pH 5, a significant 70% (*S*) e.e. was obtained in the reduction of quinaldine **B**.

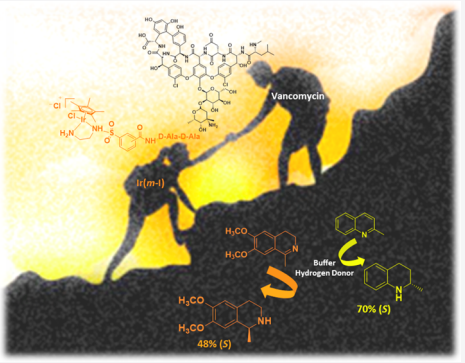

INTRODUCTION

Coordination catalysis relies on a large selection of metal ions, ligands, and substrates to achieve wide reactivity. Very sophisticated ligands have been developed, but their multistep and often challenging synthesis presents significant economic and time-demand concerns, limiting their availability. Hybrid catalysts constitute an original approach for catalysis, allowing high selectivity and specificity combined with a wide scope of reactivity and substrates. One of the bioinspired methodologies for the development of hybrid catalysts consists of the incorporation of coordination metal complexes (*i.e.,* a metal center bound to synthetic ligands) into host biomolecules, leading to the so-called artificial metalloenzymes. In these systems, the reaction is performed by the metal complex but is modulated by the well-defined structure of the biomolecule. This class of synthetic biocatalysts is particularly attractive because they combine both the features of enzymatic and transition metal catalysis. This synergistic effect conveys an added value to the catalyst such as high chemo- or enantioselectivity.[1] By analyzing metalloenzymes from a structural point of view, the first, second, and outer coordination spheres appear to play a crucial role in tuning the reactivity of the metallic center. This concept has found very large applicability in the "Trojan horse strategy" based on the covalent attachment of the organometallic moiety to a substrate that shows high affinity for the host scaffold. The main example of this strategy is the exploitation of the supramolecular biotin-(strept)avidin interaction in which a biotinylated diamine ligand in coordination with a transition metal center was anchored to a streptavidin mutant and employed as an artificial imine reductase in the stereoselective reduction of imines.[2−7]

Vancomycin (Van) is a glycopeptide antibiotic used as a last resort to effectively treat methicillin-resistant *Staphylococcus aureus* (MRSA) infections. The mode of action of Van involves the selective binding of the antibiotic to the D-Ala-D-Ala (DADA) sequence of the bacterial cell wall peptidoglycan,[8−11] leading to an inhibition of cell growth and eventual cell death. The H-bond interactions between Van and DADA (Figure 1) are particularly tight, with a dissociation constant (K_d) of 4×10^{-17} M, that is, ca. 3 orders of magnitude higher than biotin/avidin.[12−15]

The Van/DADA complex is particularly intriguing not only because of the strength of the interaction but also because of the different types of chirality arising upon its formation, due both to the presence of the aminoacidic chains and the atropoisomerism induced by the restricted rotation around the aryl−aryl bonds, a substantial feature of their structure.[16−19]

Received: October 6, 2020
Published: February 8, 2021

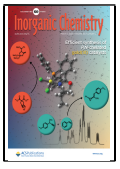

https://dx.doi.org/10.1021/acs.inorgchem.0c02969
Inorg. Chem. 2021, 60, 2976−2982

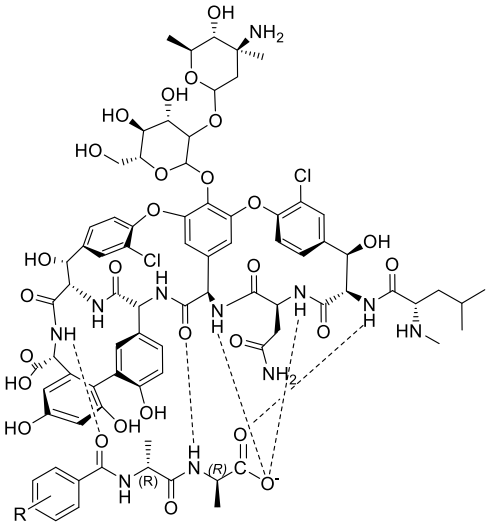

Figure 1. H-bond interactions between Van and DADA.

Here, we studied the possibility of using the Van/DADA interaction as an innovative supramolecular anchoring system for the development of new hybrid catalysts.[20] In particular, we developed new artificial metalloenzyme catalysts with Ir(III)-bearing ligands functionalized with the DADA sequence. Upon interaction with Van, two catalysts were obtained and tested in the asymmetric transfer hydrogenation (ATH) of standard cyclic imines to verify their potential as new artificial imine reductases.

RESULTS AND DISCUSSION

Recently, several biological effects of Van have been found to be related to its ability to bind both Cu(II) and Zn(II) metal ions under physiological/neutral conditions.[21−23] Starting from this point, in our previous work,[24] we focused our attention on the direct interaction between Van and $[IrCp^*Cl_2]_2$ to prepare a hybrid catalyst that could be used in the reduction of cyclic imines. The asymmetric reduction, performed by the Ir/Van catalyst, of 6,7-dimethoxy-1-methyl-3,4-dihydroisoquinoline proceeded with an appreciable conversion of up to 82%, although with a poor enantioselectivity (20% e.e. *R*). The best result in terms of enantioselectivity in the ATH of quinaldine was achieved by performing the reaction in an MES 1.2 M buffer at pH 5 with a significant 61% (*R*) e.e. even if the conversion remained low (35%). With the aim of expanding the efficiency of the hybrid system, we decided to exploit the selective binding of Van with the DADA dipeptide. The geometry of this complex is well defined, and the thermodynamics have been extensively described by Williams and co-workers.[25,26] The overall structure is stabilized by an extensive array of van der Waals contacts (hydrophobic contacts) within the Van binding pocket and five key H-bonds (Figure 1). Loose interactions occur when the sum of the favorable bonding interactions is sufficiently small to be counteracted by the adverse entropy of binding and when there is a relatively large amount of residual motion in the bound state between Van and DADA. Therefore, any modification in the DADA sequence can change the mode of association between Van and DADA, introducing favorable or unfavorable enthalpic terms. In particular, the effect of pH on determining the stability of the bond and the conformation of Van has been widely studied.[14,27]

In this work, we planned the functionalization of 2-aminoethyl-sulfamoylbenzamido ligands with DADA at the *N*-terminus. The possibility of introducing DADA in the ortho-, meta-, or para-position of the aromatic ring could, in principle, vary its interaction site with Van.[28−30] Indeed, the conformational structure of the spacer and, as a consequence, the distance between the catalytic metal complex within the second coordination sphere provided by the glycopeptide could change, thereby changing the stability of the entire system. This concept drove our choice in the use of different substituted aromatic rings as spacers for determining the variability in the interaction behavior between the DADA complex and Van.

Scheme 1. Synthesis of [IrCp*(*m*-I)Cl]Cl and [IrCp*(*p*-I)Cl]Cl Complexes Bearing *m*-I and *p*-I as Ligands

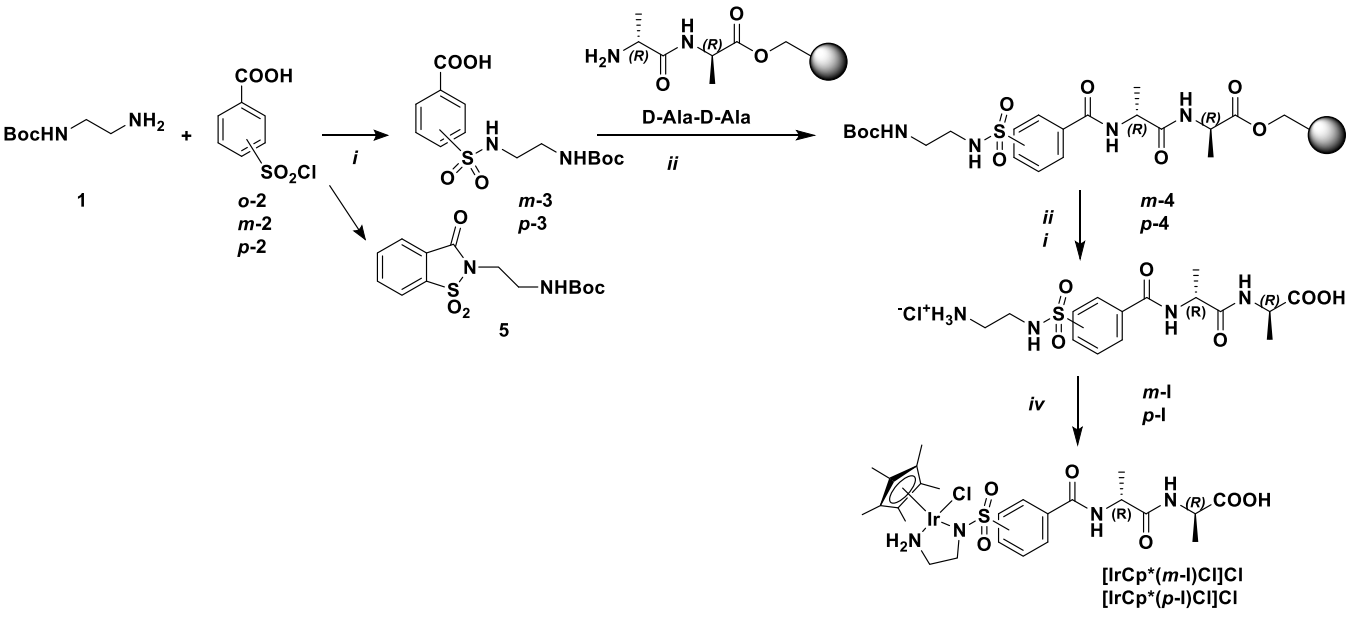

https://dx.doi.org/10.1021/acs.inorgchem.0c02969
Inorg. Chem. 2021, 60, 2976−2982

The synthesis of the ligands started from *mono*Boc-ethylenediamine that was reacted with ortho-, meta-, or para-substituted chlorosulfonyl-benzoic acids **2** (Scheme 1).

In the case of *meta*- and *para*-compounds **2**, the desired products **3** were obtained with good yield by reaction in DCM and using TEA as the base. Conversely, the *ortho*-**3** compound was never obtained, also changing the reaction conditions and the base, and in any case, only bicyclic sulfamido derivative **5** (identified by ^{1}H NMR analysis) was isolated.

The coupling between DADA and ***m*-3** and ***p*-3** was performed in the solid phase (see the Supporting Information for details).[31] Briefly, the DADA dipeptide was assembled on Wang resin using *N*-Fmoc solid-phase standard protocols;[32] then, compounds **3** were made to react with NH_2-DADA using HOBt and HBTU as coupling reagents and DIPEA as the base. After cleavage from the resin, ***m*-l** and ***p*-l** ligands were isolated with 40% overall yield. Considering the demonstrated capability of Van to coordinate directly with the iridium metal center, thus producing an effectively functioning catalyst,[33] the complexes were synthesized and used in a preformed state to avoid the possible interference derived from the direct Van/Ir interaction. The precatalysts were synthesized by dissolving the ligand ***m*-I** or ***p*-I** in 2-propanol in the presence of $[IrCp^*Cl_2]_2$ and TEA. A yellow precipitate was obtained for both ligands. The formation of the complexes was confirmed by MS, NMR analysis, and UV experiments. The UV spectra (see Figures S1 in the Supporting Information) were recorded in water (1% DMSO) at a concentration of 250 μM. For both [IrCp*(***p*-I**)Cl]Cl and [IrCp*(***m*-I**)Cl]Cl, a change in the metal-to-ligand charge transfer (MLCT) band at almost 390 nm should underline the interaction between Van and the amino acid moiety of the complex observed both using 1:1 and 2:1 ratios. This shift should be attributable to the noncovalent interactions (hydrogen bonding, $\pi-\pi$ stacking, electrostatic, hydrophobic, and van der Waals interactions) that occurred between the metal center and the second coordination sphere generated by Van around the catalytic active portion of the complex. No evidence of possible precipitation due to the increase in the amount of Van was highlighted in the spectra.[34]

A preliminary computational study was performed by evaluating the two meta- and para-systems in terms of the stability of the metal complex that was obtained. A higher stability is thus expected to lead to the favored thermodynamically stable form that has been revealed as the catalytically performing system. Models were generated starting from the aggregates of the X-ray crystal structure reported in the literature.[11,35] Four vancomycin and two DADA units were considered to retain the 2:1 ratio based on the extensive work by Chen and Loll, in which the structure of the antibiotic−target interaction was reported to always result in a dimeric ratio.[36,37] The original DADA was then modified to obtain [IrCp*(***p*-I**)H] and [IrCp*(***m*-I**)H]. The structures obtained were then optimized, employing the tight-binding GFN2-xTB method[38] including the implicit solvation model (GBSA), which has been proven to perform well in systems of this size at an affordable computational cost.[39−41] For both systems, the four possible diastereomers at the metal centers were generated with the aim of evaluating the different stabilities. The relative energy of the systems is reported in Table T2 in the Supporting Information. Among the four diastereomers, the $R_{Ir}R_{Ir}$ configuration is significantly more stable in the case of the *meta*-substituted catalyst, [IrCp*(***m*-I**)H], whereas a smaller difference between the $R_{Ir}R_{Ir}$ and $S_{Ir}R_{Ir}$ diastereomers in the case of [IrCp*(***p*-I**)H] suggests the presence of more than one diastereomer in the reaction medium. Indeed, the higher variability could be at the origin of a possible poor enantioselectivity of the *para*-system compared to the *meta*-system, as also confirmed by the catalytic results reported below. Focusing on the [IrCp*(***m*-I**)Cl]Cl ⊂ Van complex instead, the S_{Ir} configuration causes more relevant clashes between the Cp* rings of the iridium complex and the Van backbone, probably leading to the lower stability of S_{Ir}-bearing systems. (See S7−S9 in the Supporting Information). Deeper spectroscopic investigations were performed on the [IrCp*(***m*-I**)Cl]Cl ⊂ Van complex expected to be the most effective artificial metalloenzyme from the data obtained by the computational study.

2D-DOSY-^{1}H NMR experiments, performed at a final concentration of 33 mM ***m*-I** in D_2O (1.0% DMSO-d_6), indicated that Van alone in water formed aggregates (Table 1).[42−45] The increase in the calculated hydrodynamic radius

Table 1. Estimation of the Diffusion Coefficient and Hydrodynamic Radius for Van Alone and for [IrCp*(*m*-I)Cl]Cl ⊂ Van by 2D DOSY-NMR Experiments (https://www.fxsolver.com/solve/)[a]

	diffusion coefficient	hydrodynamic radius
Van	1642×10^{-10}	$148{,}859 \times 10^{-9}$
[IrCp*(***m*-I**)Cl]Cl	3725×10^{-10}	$826{,}251 \times 10^{-10}$
Van/[IrCp*(***m*-I**)Cl]Cl 1:1	2442×10^{-10}	$143{,}534 \times 10^{-9}$
Van/[IrCp*(***m*-I**)Cl]Cl 2:1	3126×10^{-10}	$206{,}418 \times 10^{-9}$

[a]DOSY-NMR: [sample] = 33 mM in D_2O (1.0% DMSO-d_6), little delta: 5.000 m, large delta: 149.900 m.

(Table 1) of the [IrCp*(***m*-I**)Cl]Cl complex in the presence of 1 equiv of Van unequivocally established the formation of the supramolecular interaction between the complex and Van (only supposed previously by UV analysis), further prompted by the increase in the equivalents of Van. (See Supporting Information, Figures S3−S6).

CD experiments were carried out in pure water and in NaOAc buffer (0.1 M, pH 5). In both cases, the presence of a positive band at 350 nm, together with a slightly positive shoulder at approximately 415 nm, both ascribable to iridium energetic transitions, confirmed the induction of chirality at the metal complex due to the presence of the second coordination sphere provided by the chiral Van moiety (Figure 2). As suggested by computational studies and by comparing the CD spectra of the [IrCp*(***m*-I**)Cl]Cl complex with the spectrum of the [IrCp*(***m*-I**)Cl]Cl ⊂ Van artificial metalloenzyme, this induced chirality is ascribable to the binding of one of the preferential configurations to Van during the supramolecular interaction transition state. This consideration was confirmed by catalysis data: when the [IrCp*(***m*-I**)Cl] complex was used alone as the catalyst without the addition of Van. The reaction proceeded to a conversion of almost 60% in 18 h without enantioselectivity. (See Supporting Information, Table T1, entries 6−11). Looking at the aromatic ring band at 285 nm, a different behavior in the CD spectra is observed depending on the environment.[46] (Figure 2) For Van alone, this band is negative, with a different intensity depending on the solvent, thus confirming the Van aggregation propensity observed in 2D-DOSY-^{1}H NMR experiments (ratio 2:1). In the [IrCp*(***m*-I**)Cl]Cl ⊂ Van artificial metalloenzyme, this band became less

https://dx.doi.org/10.1021/acs.inorgchem.0c02969
Inorg. Chem. 2021, 60, 2976−2982

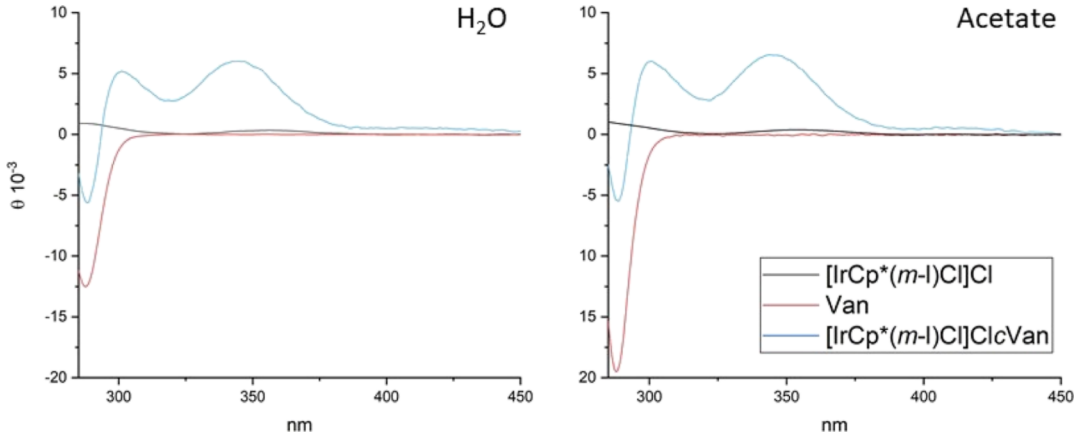

Figure 2. CD spectra of [IrCp*(***m***-I)Cl]Cl and [IrCp*(***m***-I)Cl]Cl ⊂ Van in water and acetate (2.5 mM concentration, 25 °C).

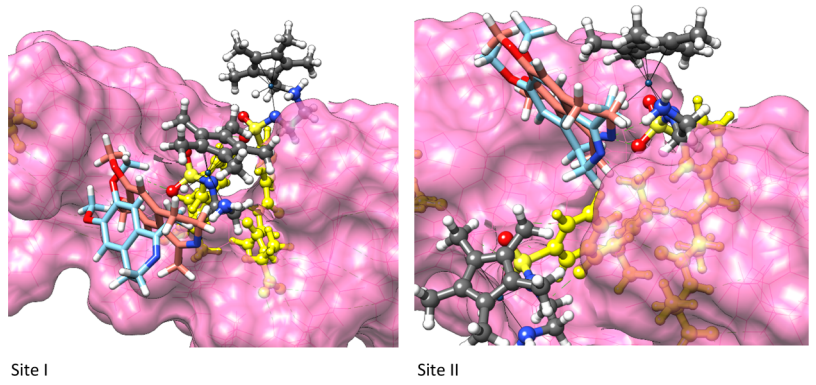

Figure 3. Computational model of the (R_{Ir},R_{Ir})-[IrCp*(***m***-I)H] ⊂ Van aggregates bound to the **A** substrate. In the left panel, the site marked as I is represented in both the pro-*R* (light blue) and pro-*S* (light red) configurations. In the right panel, site II is represented with the pro-*R* (light blue) and pro-*S* (light red) configurations. The Van molecules are represented as pink solvent-excluded molecular surfaces, and the benzamido DADAs are represented in yellow ball-and-stick representation.

intense and had the same intensity both in water and in the buffer. We can thus postulate that a change in the conformational arrangement of the aromatic rings occurred upon Van interaction with DADA, hampering its aggregation. The binding of ligands and the dimerization of vancomycin are well known to be cooperative processes. Vancomycin readily self-associates in solution, preferentially forming back-to-back dimers until the formation of a hexameric cluster.[36] The presence of certain ligands could promote the formation of face-to-face dimers involving the aromatic ring of L-phenylglycine present in the glycosylated heptapeptide. To a lesser extent is the formation of side-to-side dimers, but together, the different types of dimers may lead to the formation of large-scale vancomycin-ligand aggregates.[13,16,20,36] As evidenced by analytical characterization of our system (2D-DOSY-^{1}H NMR experiments and CD spectra), the formation of the [IrCp*(***m***-I)Cl]Cl ⊂ Van artificial metalloenzyme was highlighted even if the question of how ligand binding is correlated with the steric effect due to the different types of formed dimers has only in part been explained by the computational studies presented here.

[IrCp*(***m***-I)Cl]Cl and [IrCp*(***p***-I)Cl]Cl complexes were then used as precatalysts in the ATH of imines. A preliminary screening of the ATH reduction of substrate **A**, the precursor of salsolidine, was performed under different reaction conditions (for major information about the screening study, see Supporting Information, Table T1).[47,48] These systems were indeed particularly sensitive to many experimental parameters such as activation time, reaction temperature, substrate concentration, and substrate/catalyst ratio and buffer. In particular, as evidenced in our previous work,[24] Van should create a different chiral coordination sphere depending on the pH, ionic strength, and buffer, influencing the catalytic performance of the entire system (for additional catalytic data under different reaction conditions, see Table T1 in the Supporting Information).[33] From these preliminary screening data, we found that [IrCp*(***p***-I)Cl]Cl ⊂ Van did not perform ATH reduction in an enantioselective manner under all the reaction conditions tested, confirming the preliminary computational study results.

A deeper investigation was performed to confirm the differences in the performance of [IrCp*(***m***-I)Cl]Cl ⊂ Van in comparison to the [IrCp*(***p***-I)Cl]Cl ⊂ Van system (Figure 3). In the case of the most stable $R_{Ir}R_{Ir}$ of [IrCp*(***m***-I)H] ⊂ Van, indeed, the potential binding mode with substrate **A** was evaluated in silico. The substrate was manually docked considering the possible orientations (pro-*R* or pro-*S* configuration) in both catalytic sites. One of the two sites was revealed to be more accessible to the substrate (marked as site II in Figure S5); here, both pro-*R* and pro-*S* structures were found at low energy and distances compatible with the catalytic center; nevertheless, the pro-*S* configuration has a structure more suitable for hydrogen transfer with H···C═N distances 0.8 å shorter than those distances in pro-*R* and N···

https://dx.doi.org/10.1021/acs.inorgchem.0c02969
Inorg. Chem. 2021, 60, 2976−2982

H−N at a distance suitable for hydrogen bonding (Figure S5 and Table T3 in the Supporting Information). However, in the more hindered site I, only the interaction in the pro-*S* configuration seems to be allowed.

Then, the same analysis was performed on the two most stable diastereomers of [IrCp*(**p-I**)Cl]Cl ⊂ Van (R_{Ir},R_{Ir}) and (R_{Ir},S_{Ir}), and the results are reported in Figures S12 and S13 and Tables S4 and S5 in the Supporting Information. In the most stable form (R_{Ir},R_{Ir}), the two active sites show different preferred interactions: in site I, pro-*R* is the favorite interaction, whereas in site II, only the pro-*S* form has a structure suitable for hydrogen transfer. The outcome seems even less selective for the (R_{Ir},S_{Ir}) diastereomer, where hindered site I seems to be inaccessible to the substrate in an orientation suitable for hydrogen transfer and, at least at the level of accuracy employed here, the more exposed site II does not distinguish between the two prochiral faces of the substrate.

The results obtained in the reduction of substrate **A** were compared to two other standard cyclic imines, **B** and **C**, which are different in their electronic properties. Many buffers at different concentrations were evaluated (data not reported for all the substrates, for more information see T1 in the Supporting Information), and the best results are summarized in Table 2.

Table 2. ATH of Cyclic Imines with [IrCp*(*m*-I)Cl]Cl ⊂ Van

		u1	
entry	substrate	buffer	conv. % (e.e. %)
1	**A**	phosphate 0.1 M pH 8	16 (rac)
2	**A**	MOPS 1.2 M pH 7.8	64 (12 *S*)
3	**A**	MES 1.2 M pH 7	60 (41 *S*)
4	**A**	MES 1.2 M pH 6	96 (31 *S*)
5	**A**	CH_3COONa 0.1 M pH 5	≫99 (48 *S*)
6	**B**	phosphate 0.1 M pH 8	64 (34 *S*)
7	**B**	MOPS 1.2 M pH 7.8	32 (32 *S*)
8	**B**	MES 1.2 M pH 7	85 (51 *S*)
9	**B**	MES 1.2 M pH 6	96 (53 *S*)
10	**B**	CH_3COONa 0.1 M pH 5	76 (70 *S*)
11	**C**	phosphate 0.1 M pH 8	50 (17 *R*)
12	**C**	MOPS 1.2 M pH 7.8	57 (12 *R*)
13	**C**	MES 1.2 M pH 7	47 (27 *R*)
14	**C**	MES 1.2 M pH 6	52 (33 *R*)
15	**C**	CH_3COONa 0.1 M pH 5	48 (35 *R*)

All reactions were carried out for 18 h at 10 °C using 2 mol % [IrCp*(***m*-I**)Cl]Cl in buffer with 6 M HCOONa in all the buffers, $[sub]_f$ = 16 mM, $[cat]_f$ = 0.32 mM, Van 4 mol %. Conversion was obtained by HPLC using correction factors of 1.32 for **A** and 1.23 for **B** and **C** at λ = 283 nm. Enantiomeric excess was determined using HPLC equipped with a chiral OD-H column.[24]

CH_3COONa buffer (0.1 M pH 5) resulted as the best reaction medium: an encouraging 48% (*S*) e.e. was obtained in the asymmetric reduction of both the salsolidine precursor 6,7-dimethoxy-1-methyl-3,4-dihydroisoquinoline **A** and 35% (*R*) e.e. in the reduction of the pharmacologically interesting sultam precursor[49] 3-methylbenzo[*d*]isothiazole-1,1-dioxide **C** (Table 2, entries 5 and 15). An appreciable 70% (*S*) e.e. was obtained in the reduction of quinaldine **B** (Table 2, entry 10). In all cases, the best results were obtained using CH_3COONa buffer, pH 5 at 10 °C, confirming the pH dependence of the catalytic system on the hybrid system performance. Focusing on the pH and both the conversion % and the e.e. %, a clear correlation for all the substrates, as evidenced by the graphics reported in the Supporting Information (see Supporting Information, Figure S3), was confirmed both at pH 6 and 5, resulting, in all cases, in the best reaction conditions in which the reactions were conducted. Considering that the ionic strength decreases as a function of the buffer (phosphate F_i 0.95/pH 8, MES and MOPS F_i 0.6/pH 7.8, 7, and 6, and CH_3COONa F_i 0.1/pH 5), the results obtained with MES (F_i 0.6) and CH_3COONa (F_i 0.1) underlined that, in contrast to those of our system, the ionic strength was not as significant. One of the parameters considered in the preliminary screening was the H_2 donor/substrate ratio. Considering that the H_2 donor (HCOONa) could influence the ionic strength as a function of its concentration, a relationship between the ratio and both the conversion % and e.e. % was analyzed. As highlighted by the graphic reported in the Supporting Information (see Supporting Information, Figure S4), with respect to e.e. %, there are not so many differences, but the conversion result is lower for ratio 5/1, probably due more to the decrease in availability of hydride in the reaction system than to its contribution to the ionic strength. An increase in the reaction temperature and/or in the pH of buffer indeed led to a decrease in the enantioselectivity, probably due to a decreasing rigidity of the Van scaffold around the metal complex. From these findings, the major impact of the second sphere in inducing chirality in the system is evicted, as underlined by the increase in enantioselectivity in the presence of Van. Interesting was the comparison between the results obtained for the Van/Ir hybrid system (Van directly coordinated with the iridium center)[24] in which the products of substrates **A** and **B** were in the *R* configuration and of **C** in the *S* configuration and the artificial metalloenzyme in which the configuration for all the products was inverted. This aspect shed light on the complementary behavior of the two different coordination modes around the metal center (direct and supramolecular) of Van in obtaining both enantiomers. The system proposed here was comparable to the other metalloenzymes reported in the literature and used as catalysts for the ATH reaction of salsolidine precursors. In particular, the metalloenzyme based on streptavidine/biotin technology, previously studied by our group,[28,29] confirmed the possibility of creating a real chiral catalyst starting from an achiral metal complex. The Van/DADA system was more sensitive to variations in pH values than the other systems, indicating an interesting change in the conformational arrangement of Van and the consequent loss of chirality of the entire catalytic system.

CONCLUSIONS

In conclusion, two new artificial imine reductases based on the supramolecular interaction between Van and an opportunely modified DADA−iridium complex were synthesized and used as catalysts in the ATH of standard cyclic imines. The system bearing the ligand ***m*-I** was more efficient in terms of both regio- and enantioselectivity than the ***p*-I** ligand. The [IrCp*(***m*-I**)Cl]Cl ⊂ Van artificial metalloenzyme was fully characterized by CD and 2D-DOSY-^{1}H NMR experiments, confirming the supramolecular interaction between the metal complex and the biological scaffold. The computational studies confirmed this behavior and allowed us to characterize the

https://dx.doi.org/10.1021/acs.inorgchem.0c02969
Inorg. Chem. 2021, 60, 2976−2982

more stable and catalytically performing system. The [IrCp*-(*m*-**I**)Cl]Cl ⊂ Van reduced quinaldine **B** in a good 76% conversion with an appreciable 70% e.e. for the enantiomer in the *S* configuration. Starting from the assumption that the dimer DADA is essential and therefore unchangeable, another future strategy could be the use of well-known modified glycopeptide structures synthesized to overcome resistance issues.

EXPERIMENTAL SECTION

General. Vancomycin was commercially available. $[IrCp^*Cl_2]_2$ was synthesized as reported in the literature.[50] Catalytic reactions were monitored by HPLC analysis with a Merck-Hitachi L-7100 equipped with a Detector UV6000 LP and chiral column (Chiralcel OD-H). HRMS analyses were performed by using a QTof Synapt G2 Si spectrometer with an electrospray ionization source. The spectra were obtained by direct infusion of a sample solution in MeOH under ionization, ESI positive. ^1H and ^{13}C NMR spectra were recorded in $D_2O/[d_6]DMSO$ (1% v/v) on a Bruker AVANCE 600 MHz. Chemical shift (δ) is expressed in parts per million (ppm). All experiments were recorded at 298 K using TMS as an internal standard.

General Procedure for ATH. [IrCp*(**I**)Cl]Cl (2% mol) and Van (4% mol) were dissolved in 1 mL of buffer (HCOONa 6 M, final pH 5, 6, 7, 7.8 or 8) and stirred for 30 min at 25 °C. The substrate (final concentration 16 mM) was added to the catalyst solution. The reaction was stirred for 18 h at 10 °C. At the end of the reaction, 10 μL of 10 N NaOH was added, and the aqueous medium was extracted with CH_2Cl_2 for substrates **A** and **B** and with ethyl acetate for substrate **C**. The organic layers were dried with anhydrous Na_2SO_4 and filtered, and the solvent was removed under vacuum for analysis by an HPLC equipped with a chiral column to determine conversion and enantiomeric excess.[24]

ASSOCIATED CONTENT

Supporting Information

The Supporting Information is available free of charge at https://pubs.acs.org/doi/10.1021/acs.inorgchem.0c02969.

UV-vis spectra; CD spectra; preliminary screening for substrate A; graphics of relationship between the pH and both the conversion % and the e.e. % for all the substrates; graphic of relationship between the H_2 donor/substrate ratio and both the conversion % and the e.e. % for all the substrates; 2D-DOSY-^{1}H-NMR experiments; relative stability of the aggregates; computational models; and relative stability of the aggregates (PDF)

AUTHOR INFORMATION

Corresponding Authors

Sara Pellegrino − *Dipartimento di Scienze Farmaceutiche, Università degli Studi di Milano, 20133 Milano, Italy;* orcid.org/0000-0002-2325-3583; Email: sara.pellegrino@unimi.it

Isabella Rimoldi − *Dipartimento di Scienze Farmaceutiche, Università degli Studi di Milano, 20133 Milano, Italy;* orcid.org/0000-0002-6210-0264; Email: Isabella.rimoldi@unimi.it

Authors

Giorgio Facchetti − *Dipartimento di Scienze Farmaceutiche, Università degli Studi di Milano, 20133 Milano, Italy;* orcid.org/0000-0002-1260-1335

Raffaella Bucci − *Dipartimento di Scienze Farmaceutiche, Università degli Studi di Milano, 20133 Milano, Italy*

Marco Fusè − *Scuola Normale Superiore, 56126 Pisa, Italy;* orcid.org/0000-0003-0130-5175

Emanuela Erba − *Dipartimento di Scienze Farmaceutiche, Università degli Studi di Milano, 20133 Milano, Italy*

Raffaella Gandolfi − *Dipartimento di Scienze Farmaceutiche, Università degli Studi di Milano, 20133 Milano, Italy;* orcid.org/0000-0003-2145-8574

Complete contact information is available at: https://pubs.acs.org/10.1021/acs.inorgchem.0c02969

Author Contributions

§G.F. and R.B. contributed equally.

Notes

The authors declare no competing financial interest.

REFERENCES

(1) Lewis, J. C. Artificial Metalloenzymes and Metallopeptide Catalysts for Organic Synthesis. *ACS Catal.* **2013**, *3*, 2954−2975.

(2) Heinisch, T.; Pellizzoni, M.; Dürrenberger, M.; Tinberg, C. E.; Köhler, V.; Klehr, J.; Häussinger, D.; Baker, D.; Ward, T. R. Improving the Catalytic Performance of an Artificial Metalloenzyme by Computational Design. *J. Am. Chem. Soc.* **2015**, *137*, 10414−10419.

(3) Pàmies, O.; Diéguez, M.; Bäckvall, J.-E. Artificial Metalloenzymes in Asymmetric Catalysis: Key Developments and Future Directions. *Adv. Synth. Catal.* **2015**, *357*, 1567−1586.

(4) Schwizer, F.; Okamoto, Y.; Heinisch, T.; Gu, Y.; Pellizzoni, M. M.; Lebrun, V.; Reuter, R.; Köhler, V.; Lewis, J. C.; Ward, T. R. Artificial Metalloenzymes: Reaction Scope and Optimization Strategies. *Chem. Rev.* **2018**, *118*, 142−231.

(5) Lin, Y.-W. Rational design of metalloenzymes: From single to multiple active sites. *Coord. Chem. Rev.* **2017**, *336*, 1−27.

(6) Hyster, T. K.; Ward, T. R. Genetic Optimization of Metalloenzymes: Enhancing Enzymes for Non-Natural Reactions. *Angew. Chem., Int. Ed.* **2016**, *55*, 7344−7357.

(7) Hestericová, M.; Heinisch, T.; Alonso-Cotchico, L.; Maréchal, J.-D.; Vidossich, P.; Ward, T. R. Directed Evolution of an Artificial Imine Reductase. *Angew. Chem., Int. Ed.* **2018**, *57*, 1863−1868.

(8) McComas, C. C.; Crowley, B. M.; Boger, D. L. Partitioning the Loss in Vancomycin Binding Affinity for d-Ala-d-Lac into Lost H-Bond and Repulsive Lone Pair Contributions. *J. Am. Chem. Soc.* **2003**, *125*, 9314−9315.

(9) Rao, J.; Whitesides, G. M. Tight Binding of a Dimeric Derivative of Vancomycin with Dimeric l-Lys-d-Ala-d-Ala. *J. Am. Chem. Soc.* **1997**, *119*, 10286−10290.

(10) Rao, J.; Lahiri, J.; Weis, R. M.; Whitesides, G. M. Design, Synthesis, and Characterization of a High-Affinity Trivalent System Derived from Vancomycin and l-Lys-d-Ala-d-Ala. *J. Am. Chem. Soc.* **2000**, *122*, 2698−2710.

(11) Nitanai, Y.; Kikuchi, T.; Kakoi, K.; Hanamaki, S.; Fujisawa, I.; Aoki, K. Crystal Structures of the Complexes between Vancomycin and Cell-Wall Precursor Analogs. *J. Mol. Biol.* **2009**, *385*, 1422−1432.

(12) McPhail, D.; Cooper, A. Thermodynamics and kinetics of dissociation of ligand-induced dimers of vancomycin antibiotics. *J. Chem. Soc., Faraday Trans.* **1997**, *93*, 2283−2289.

(13) Rekharsky, M.; Hesek, D.; Lee, M.; Meroueh, S. O.; Inoue, Y.; Mobashery, S. Thermodynamics of Interactions of Vancomycin and Synthetic Surrogates of Bacterial Cell Wall. *J. Am. Chem. Soc.* **2006**, *128*, 7736−7737.

(14) Xing, B.; Jiang, T.; Wu, X.; Liew, R.; Zhou, J.; Zhang, D.; Yeow, E. K. L. Molecular Interactions between Glycopeptide Vancomycin and Bacterial Cell Wall Peptide Analogues. *Chem.—Eur. J.* **2011**, *17*, 14170−14177.

(15) Rao, J.; Lahiri, J.; Isaacs, L.; Weis, R. M.; Whitesides, G. M. A Trivalent System from Vancomycin·d-Ala-d-Ala with Higher Affinity Than Avidin·Biotin. *Science* **1998**, *280*, 708−711.

(16) Jia, Z.; O'Mara, M. L.; Zuegg, J.; Cooper, M. A.; Mark, A. E. Vancomycin: ligand recognition, dimerization and super-complex formation. *FEBS J.* **2013**, *280*, 1294−1307.
(17) Pearce, C. M.; Williams, D. H. Complete assignment of the 13C NMR spectrum of vancomycin. *J. Chem. Soc., Perkin Trans. 2* **1995**, *2*, 153−157.
(18) Facchetti, G.; Cesarotti, E.; Pellizzoni, M.; Zerla, D.; Rimoldi, I. "In situ" Activation of Racemic RuII Complexes: Separation of trans and cis Species and Their Application in Asymmetric Reduction. *Eur. J. Inorg. Chem.* **2012**, *2012*, 4365−4370.
(19) Fusè, M.; Rimoldi, I.; Facchetti, G.; Rampino, S.; Barone, V. Exploiting coordination geometry to selectively predict the σ-donor and π-acceptor abilities of ligands: a back-and-forth journey between electronic properties and spectroscopy. *Chem. Commun.* **2018**, *54*, 2397−2400.
(20) Loll, P. J.; Derhovanessian, A.; Shapovalov, M. V.; Kaplan, J.; Yang, L.; Axelsen, P. H. Vancomycin Forms Ligand-Mediated Supramolecular Complexes. *J. Mol. Biol.* **2009**, *385*, 200−211.
(21) Nair, U. B.; Chang, S. S. C.; Armstrong, D. W.; Rawjee, Y. Y.; Eggleston, D. S.; McArdle, J. V. Elucidation of vancomycin's enantioselective binding site using its copper complex. *Chirality* **1996**, *8*, 590−595.
(22) Swiatek, M.; Valensin, D.; Migliorini, C.; Gaggelli, E.; Valensin, G.; Jezowska-Bojczuk, M. Unusual binding ability of vancomycin towards Cu2+ ions. *Dalton Trans.* **2005**, 3808−3813.
(23) Zarkan, A.; Macklyne, H.-R.; Truman, A. W.; Hesketh, A. R.; Hong, H.-J. The frontline antibiotic vancomycin induces a zinc starvation response in bacteria by binding to Zn(II). *Sci. Rep.* **2016**, *6*, 19602.
(24) Facchetti, G.; Pellegrino, S.; Bucci, R.; Nava, D.; Gandolfi, R.; Christodoulou, M. S.; Rimoldi, I. Vancomycin-Iridium (III) Interaction: An Unexplored Route for Enantioselective Imine Reduction. *Molecules* **2019**, *24*, 2771.
(25) Sheldrick, G. M.; Jones, P. G.; Kennard, O.; Williams, D. H.; Smith, G. A. Structure of vancomycin and its complex with acetyl-D-alanyl-D-alanine. *Nature* **1978**, *271*, 223−225.
(26) Williamson, M. P.; Williams, D. H. Structure revision of the antibiotic vancomycin. Use of nuclear Overhauser effect difference spectroscopy. *J. Am. Chem. Soc.* **1981**, *103*, 6580−6585.
(27) Popieniek, P. H.; Pratt, R. F. Kinetics and mechanism of binding of specific peptides to vancomycin and other glycopeptide antibiotics. *J. Am. Chem. Soc.* **1991**, *113*, 2264−2270.
(28) Pellizzoni, M.; Facchetti, G.; Gandolfi, R.; Fusè, M.; Contini, A.; Rimoldi, I. Evaluation of Chemical Diversity of Biotinylated Chiral 1,3-Diamines as a Catalytic Moiety in Artificial Imine Reductase. *ChemCatChem* **2016**, *8*, 1665−1670.
(29) Facchetti, G.; Rimoldi, I. 8-Amino-5,6,7,8-tetrahydroquinoline in iridium(iii) biotinylated Cp* complex as artificial imine reductase. *New J. Chem.* **2018**, *42*, 18773−18776.
(30) Pellegrino, S.; Facchetti, G.; Contini, A.; Gelmi, M. L.; Erba, E.; Gandolfi, R.; Rimoldi, I. Ctr-1 Mets7 motif inspiring new peptide ligands for Cu(i)-catalyzed asymmetric Henry reactions under green conditions. *RSC Adv.* **2016**, *6*, 71529−71533.
(31) Bucci, R.; Giofré, S.; Clerici, F.; Contini, A.; Pinto, A.; Erba, E.; Soave, R.; Pellegrino, S.; Gelmi, M. L. Tetrahydro-4H-(pyrrolo[3,4-d]isoxazol-3-yl)methanamine: A Bicyclic Diamino Scaffold Stabilizing Parallel Turn Conformations. *J. Org. Chem.* **2018**, *83*, 11493−11501.
(32) Macut, H.; Hu, X.; Tarantino, D.; Gilardoni, E.; Clerici, F.; Regazzoni, L.; Contini, A.; Pellegrino, S.; Luisa Gelmi, M. Tuning PFKFB3 Bisphosphatase Activity Through Allosteric Interference. *Sci. Rep.* **2019**, *9*, 20333.
(33) Facchetti, G.; Pellegrino, S.; Bucci, R.; Nava, D.; Gandolfi, R.; Christodoulou, M. S.; Rimoldi, I. Vancomycin-Iridium (III) Interaction: An Unexplored Route for Enantioselective Imine Reduction. *Molecules* **2019**, *24*, 2771.
(34) Barker, K. D.; Eckermann, A. L.; Sazinsky, M. H.; Hartings, M. R.; Abajian, C.; Georganopoulou, D.; Ratner, M. A.; Rosenzweig, A. C.; Meade, T. J. Protein Binding and the Electronic Properties of Iron(II) Complexes: An Electrochemical and Optical Investigation of Outer Sphere Effects. *Bioconjugate Chem.* **2009**, *20*, 1930−1939.
(35) Schäfer, M.; Schneider, T. R.; Sheldrick, G. M. Crystal structure of vancomycin. *Structure* **1996**, *4*, 1509−1515.
(36) Cheng, M.; Ziora, Z. M.; Hansford, K. A.; Blaskovich, M. A.; Butler, M. S.; Cooper, M. A. Anti-cooperative ligand binding and dimerisation in the glycopeptide antibiotic dalbavancin. *Org. Biomol. Chem.* **2014**, *12*, 2568−2575.
(37) Economou, N. J.; Nahoum, V.; Weeks, S. D.; Grasty, K. C.; Zentner, I. J.; Townsend, T. M.; Bhuiya, M. W.; Cocklin, S.; Loll, P. J. A Carrier Protein Strategy Yields the Structure of Dalbavancin. *J. Am. Chem. Soc.* **2012**, *134*, 4637−4645.
(38) Bannwarth, C.; Ehlert, S.; Grimme, S. GFN2-xTB—An Accurate and Broadly Parametrized Self-Consistent Tight-Binding Quantum Chemical Method with Multipole Electrostatics and Density-Dependent Dispersion Contributions. *J. Chem. Theory Comput.* **2019**, *15*, 1652−1671.
(39) Seibert, J.; Bannwarth, C.; Grimme, S. Biomolecular Structure Information from High-Speed Quantum Mechanical Electronic Spectra Calculation. *J. Am. Chem. Soc.* **2017**, *139*, 11682−11685.
(40) Pracht, P.; Bohle, F.; Grimme, S. Automated exploration of the low-energy chemical space with fast quantum chemical methods. *Phys. Chem. Chem. Phys.* **2020**, *22*, 7169−7192.
(41) Bohle, F.; Grimme, S., Efficient structural and energetic screening of fullerene encapsulation in a large supramolecular double decker macrocycle. **2019** 2019, *84* (), 837. DOI: 10.2298/jsc190701079b
(42) Neufeld, R.; Stalke, D. Accurate molecular weight determination of small molecules via DOSY-NMR by using external calibration curves with normalized diffusion coefficients. *Chem. Sci.* **2015**, *6*, 3354−3364.
(43) Brune, D.; Kim, S. Predicting protein diffusion coefficients. *Proc. Natl. Acad. Sci. U.S.A.* **1993**, *90*, 3835−3839.
(44) Valencia, D. P.; González, F. J. Understanding the linear correlation between diffusion coefficient and molecular weight. A model to estimate diffusion coefficients in acetonitrile solutions. *Electrochem. Commun.* **2011**, *13*, 129−132.
(45) Rimoldi, I.; Facchetti, G.; Cesarotti, E.; Pellizzoni, M.; Fuse, M.; Zerla, D. Enantioselective transfer hydrogenation of aryl ketones: synthesis and 2D-NMR characterization of new 8-amino-5,6,7,8-tetrahydroquinoline Ru(II)-complexes. *Curr. Org. Chem.* **2012**, *16*, 2982−2988.
(46) Nieto, M.; Perkins, H. R. Physicochemical properties of vancomycin and iodovancomycin and their complexes with diacetyl-l-lysyl-d-alanyl-d-alanine. *Biochem. J.* **1971**, *123*, 773−787.
(47) Facchetti, G.; Bucci, R.; Fusè, M.; Rimoldi, I. Asymmetric Hydrogenation vs Transfer Hydrogenation in the Reduction of Cyclic Imines. *ChemistrySelect* **2018**, *3*, 8797−8800.
(48) Vilhanová, B.; Václavík, J.; Šot, P.; Pecháček, J.; Zápal, J.; Pažout, R.; Maixner, J.; Kuzma, M.; Kačer, P. Enantioselective hydrogenation of cyclic imines catalysed by Noyori-Ikariya half-sandwich complexes and their analogues. *Chem. Commun.* **2016**, *52*, 362−365.
(49) Li, Y.; Lei, M.; Yuan, W.; Meggers, E.; Gong, L. An N-heterocyclic carbene iridium catalyst with metal-centered chirality for enantioselective transfer hydrogenation of imines. *Chem. Commun.* **2017**, *53*, 8089−8092.
(50) Zerla, D.; Facchetti, G.; Fusè, M.; Pellizzoni, M.; Castellano, C.; Cesarotti, E.; Gandolfi, R.; Rimoldi, I. 8-Amino-5,6,7,8-tetrahydroquinolines as ligands in iridium(III) catalysts for the reduction of aryl ketones by asymmetric transfer hydrogenation (ATH). *Tetrahedron: Asymmetry* **2014**, *25*, 1031−1037.

https://dx.doi.org/10.1021/acs.inorgchem.0c02969
Inorg. Chem. 2021, 60, 2976−2982